Phase shifting digital holography implemented with a twisted-nematic liquid-crystal display

Maria-Luisa Cruz, Albertina Castro, and Victor Arrizón*

Instituto Nacional de Astrofísica, Optica y Electrónica, Apartado Postal 51 y 216, Puebla, PUE 72000, México

*Corresponding author: arrizon@inaoep.mx

Received 27 July 2009; revised 18 November 2009; accepted 18 November 2009; posted 19 November 2009 (Doc. ID 114732); published 10 December 2009

We describe and experimentally demonstrate a phase shifting method based on the lateral displacement of a grating implemented with a twisted-nematic liquid-crystal spatial light modulator. This method allows an accurate implementation of the phase shift without requiring moving parts. The technique is implemented in a Mach–Zehnder digital holography setup in which the field transmitted by the sample object freely propagates to the hologram plane. © 2009 Optical Society of America

OCIS codes: 090.1995, 090.1970, 120.3180, 100.5070, 180.3170.

1. Introduction

Digital holography (DH) allows the measurement of both the amplitude and the phase of a complex optical field by computer processing of digitized holograms of this field [1–8]. These holograms are recorded with electronic imaging devices, e.g., CCDs, limited by poor spatial resolution, which reduces the spatial frequency bandwidth of the complex fields that can be analyzed, especially if the recorded holograms employ an off-axis reference wave. This drawback is minimized by use of the phase shifting interferometry (PSI) technique [9–11], since it can be implemented with on-axis DH setups. However, PSI requires at least two holograms of the studied field that must be recorded under high mechanical stability of the optical setup. In addition, this technique requires a controlled phase shift between the reference beam and the object field that interfere to form each hologram. In general an accurate realization of this phase shift is not an obvious task, especially when the number of phase steps is four or more. A simplified and convenient version of PSI is the one that employs only two phase levels [12,13].

PSI is usually implemented by means of piezoelectric transducers [9–11] or, alternately, by employing passive or electro-optic phase plates [14–17]. We describe a two-step PSI method for DH based on the lateral displacement of a binary grating, which is generated by a twisted-nematic liquid-crystal (TNLC) spatial light modulator (SLM). A laser beam that illuminates this grating is transformed into several beams from which the first-order beam is employed as the reference wave. If the grating is laterally displaced, this beam is affected by a phase shift that is proportional to the displacement. This implementation of the phase shift is accurate since the required lateral displacement of the grating is simply performed by changing the image displayed in the SLM. In this approach the exact modulation of the generated grating, which in general is complex, does not affect the accuracy of the generated phase shift. For this reason it is possible to employ a conventional TNLC SLM, which is relatively inexpensive and widely available.

The phase shifting based on the lateral displacement of a grating was previously applied in a common path interferometry setup [18,19]. However, this setup, which is based on a double-Fourier transform processor, permits analysis only of low bandwidth objects, because of the paraxial operation of the Fourier transforming lenses. We evaluate the performance

0003-6935/09/366907-06$15.00/0

of the PSI technique, based on the displacement of gratings, in a Mach–Zehnder optical setup that registers holograms of a field freely propagated from the sample object to the electronic register plane. This technique, as with any other PSI method, can recover sample objects with a relatively large bandwidth by use of on-axis holograms. This PSI method and the optical setup in which we implement it, together with the digital process for reconstruction of the analyzed complex field, are described in Section 2. An experimental demonstration of the method is reported in Section 3, and final remarks are presented in Section 4.

2. Optical Setup and the Phase Shift Technique

The optical setup that we employ to implement the PSI method is schematically depicted in Fig. 1. The beam transmitted by beam splitter BS1 arrives at the TNLC SLM, where a binary grating is generated. Lens L_1 is used to focus the multiple beams diffracted by this grating. Spatial filter SF_1 is placed at the focal plane of lens L_1, where the multiple beams appear focused, to transmit only the first-order diffracted beam generated by the grating. Lens L_2 recollimates the transmitted beam, which is employed as the reference beam. The width of this beam is controlled by the ratio f_2/f_1, where f_1 and f_2 are the focal lengths of lenses L_1 and L_2, respectively. The beam reflected by beam splitter BS_1, which is employed to illuminate the object, is expanded by the pair of lenses L_3 and L_4, and cleaned by spatial filter SF_2. The interference of the object field with the reference beam, allowed by beam splitter BS_2, is recorded by a CCD.

We assume that a binary grating with vertically oriented fringes and fundamental period p is generated by the SLM. The transmittance of this grating can be expressed by the Fourier series

$$g(x) = \sum_{n=-\infty}^{\infty} c_n \exp\left(i2\pi \frac{n}{p} x\right), \tag{1}$$

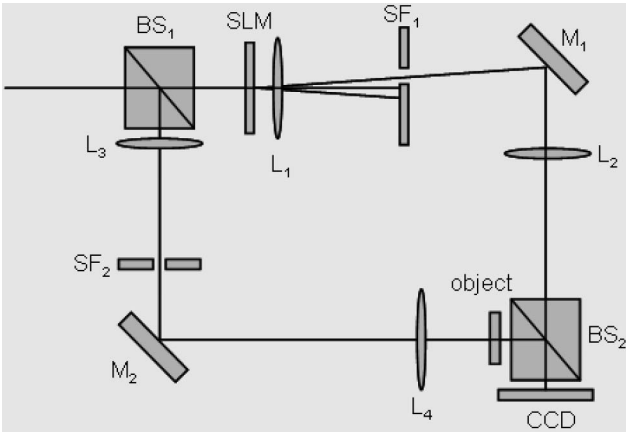

Fig. 1. Optical setup for implementation of the two-step phase shift method.

where coefficients c_n are complex constants. For this representation of the grating transmittance as a one-dimensional function we disregard the vertical modulation that is due to the pixelated SLM structure. The consideration of this feature does not provide essential differences in the results. In our experimental implementation of the PSI method, the beam that enters beam splitter BS1 (Fig. 1) is the one obtained directly from the He–Ne laser. The laser beam transmitted by this splitter arrives at the SLM with a waist radius (<2 mm) that is much smaller than the SLM width (≈ 2.5 cm). Therefore, if the complex amplitude of the laser beam that illuminates the grating is $b(x,y)$, the beam transmitted by the SLM can be expressed as $b(x,y)g(x)$, where $g(x)$ is the grating transmittance, without the necessity to introduce an explicit SLM pupil function. Considering Eq. (1) it is noted that this field is formed by multiple copies of beam $b(x,y)$, propagating in different directions. In particular, the first-order beam, whose complex amplitude at the SLM plane is

$$g_1(x,y) = c_1 b(x,y) \exp(i2\pi x/p), \tag{2}$$

is used to form the reference beam in the DH setup (Fig. 1). When we perform lateral displacement Δx in the grating loaded to the SLM, its new transmittance is given by

$$g(x-\Delta x) = \sum_{n=-\infty}^{\infty} c_n \exp\left(-i2\pi \frac{n}{p}\Delta x\right) \exp\left(i2\pi \frac{n}{p} x\right). \tag{3}$$

When this shifted grating is illuminated by beam $b(x,y)$, the new transmitted first-order beam is

$$g_2(x,y) = \exp(-i2\pi\Delta x/p)\, g_1(x,y). \tag{4}$$

As a result, lateral displacement Δx in the loaded grating introduces phase shift $\exp(-i2\pi\Delta x/p)$ in the first-order diffracted beam.

To implement the two-step PSI in the DH setup, we obtain the reference beam from the first-order beam transmitted by the grating generated with the SLM. In this PSI method, the required phase shift in the reference beam is $\exp(i\pi/2)$. According to Eq. (4), this phase shift is obtained by grating displacement $\Delta x = -p/4$. Partial views of the binary gratings uploaded to the SLM to perform the phase shift are shown in Fig. 2. The images in this figure correspond, respectively, to gratings $g(x)$ and $g(x-\Delta x)$ in Eqs. (1) and (3). Grating $g(x-\Delta x)$, whose displacement is $\Delta x = -p/4$, generates the reference beam with phase shift $\exp(i\pi/2)$. In the above derivation the result is independent of the explicit expression for grating transmittance function $g(x)$. In particular, the result is independent of the pixel pitch and pixel size of the SLM. In Section 3, a two-step phase shift is experimentally implemented loading the LC SLM with a binary grating whose period p

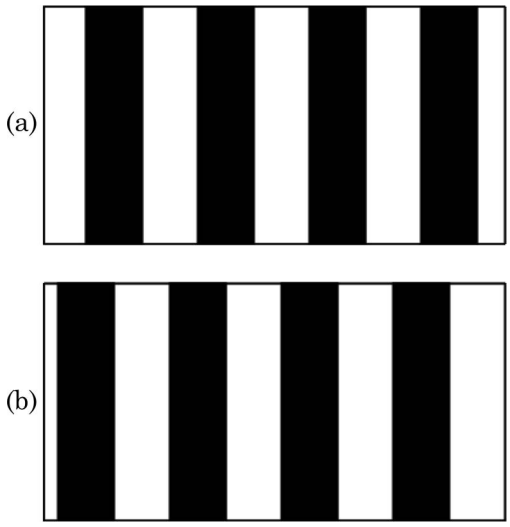

Fig. 2. Several periods of the gratings loaded to the SLM to generate phase shifts of (a) 0 and (b) $\pi/2$.

is equal to 4 SLM pixels, which correspond to the maximum possible spatial frequency that allows lateral displacement $\Delta x = -p/4$.

The focusing and isolation of the first-order beam transmitted by the SLM grating are performed, respectively, by lens L_1 and spatial filter SF_1. Since lens L_1 operates as a Fourier transform, the distance between adjacent focused beams can be much greater than the waist of these beams by simply ensuring that the beam waist, at the grating plane, is much larger than the period of this grating. Therefore, it is not difficult to isolate and transmit (practically without clipping) through an appropriate pinhole, only the first-order focused beam. Afterward, the focused reference beam is transmitted by the spatial filter and is expanded and collimated by lens L_2. A similar expansion and collimation are performed on the object beam using lenses L_3 and L_4 and spatial filter SF_2.

The complex field propagated from the object to the CCD plane is expressed as

$$o(x,y) = a(x,y)\exp[i\phi(x,y)]. \tag{5}$$

On the other hand, the complex amplitude of the reference beam at the CCD plane is given by

$$r(x,y) = a_r(x,y)\exp\{i[2\pi(u_0x + v_0y) + \delta]\}, \tag{6}$$

where δ is the phase delay controlled by the lateral displacement of the grating implemented in the SLM, and $2\pi(u_0x + v_0y)$ is a linear phase that appears if the reference beam does not propagate perfectly on axis. Phase shift $\exp(i\delta)$ that appears as a factor of the first-order beam diffracted by the SLM grating when it is laterally shifted is a constant, which is maintained during expansion, filtering, and collimation and transforms this beam into the reference field. If one considers the distortion of the beam by possible aberration of lenses L_1 and L_2, the phase factor in Eq. (6) would be transformed into $\exp\{i[2\pi(u_0x + v_0y) + w(x,y) + \delta]\}$, where $w(x,y)$ is the wave aberration at the CCD plane. In general, it is necessary to measure aberration $w(x,y)$, if it is not negligible, to eliminate it from the measured phase of the object phase. Here our main purpose is to present a demonstration of the two-step PSI implemented with a displaced grating generated with a SLM, so the analysis and compensation of aberrations that are due to the lenses is disregarded.

The intensity of the recorded hologram, obtained by the superposition of fields $o(x,y)$ and $r(x,y)$ [Eqs. (5) and (6)] is

$$\begin{aligned} I(x,y) = {} & a_r^2(x,y) + a^2(x,y) \\ & + 2a_r(x,y)a(x,y)\cos[\phi(x,y) \\ & - 2\pi(u_0x + v_0y) - \delta]. \end{aligned} \tag{7}$$

We make the reasonable assumption that amplitude $a_r(x,y)$ of the reference beam is not constant but presents nonzero values within the recording area. We have also assumed that the phase of the reference beam is close to that of a plane wave. If in addition to hologram $I(x,y)$ the intensity patterns $I_0(x,y) = a^2(x,y)$ and $I_r(x,y) = a_r^2(x,y)$ are recorded, we can compute the modified hologram $I_m = [I - I_0 - I_r]/(2I_r^{1/2})$. If we consider phase shifts $\delta = 0$ and $\delta = \pi/2$, I_m takes, respectively, the form of functions

$$I_c(x,y) = a(x,y)\cos[\phi(x,y) - 2\pi(u_0x + v_0y)], \tag{8}$$

$$I_s(x,y) = a(x,y)\sin[\phi(x,y) - 2\pi(u_0x + v_0y)]. \tag{9}$$

Considering Eqs. (8) and (9) it is shown that object field $o(x,y)$ is recovered as

$$o(x,y) = [I_c(x,y) + iI_s(x,y)]\exp[i2\pi(u_0x + v_0y)]. \tag{10}$$

We assume that the spectrum of object $o(x,y)$ is centered at origin $(0,0)$ in the Fourier plane. Therefore, factor $\exp[i2\pi(u_0x + v_0y)]$ is obtained as the linear phase modulation that must be applied to the function $I_c(x,y) + iI_s(x,y)$ to obtain its Fourier spectrum centered at the origin in the Fourier plane. The complex field at the object plane is computed by backpropagation of reconstructed field $o(x,y)$ to the object plane.

3. Experimental Implementation of the Phase Shift

We implemented the optical setup depicted in Fig. 1 using a TNLC SLM (Model LC2002, Holoeye Photonics AG, Berlin-Adlershof, Germany) with a pixel pitch of 32 μm and screen format of 600 × 800 pixels. The SLM is sandwiched between two linear polarizers that allow the operation of this device as mostly an amplitude modulator. A polarization rotator (not shown) is employed to align the polarization of the beam that illuminates the object to that of

the reference beam. We used a He–Ne laser with a wavelength of 632.8 nm as the illumination source. The holograms were recorded and digitized using a CCD (FireWire DC310, Thorlabs, Newton, New Jersey) with 1024×768 pixels and a pixel pitch of 4.7 μm.

For the first experiment we performed direct measurement of the phase shift generated with the proposed method. For this purpose we removed the sample object in the setup and tilted the reference wave slightly to obtain a sinusoidal interference pattern at the CCD plane. To generate the phase shift in the reference beam, the SLM is sequentially loaded with the two relatively displaced gratings shown in Fig. 2, with a period equal to 4 SLM pixels. The two recorded interference patterns are depicted in Fig. 3. The black lines superposed at the fringes correspond to their numerically computed intensity peaks. A unit in the spatial scale on the axes of the figure corresponds to the CCD resolution (4.7 μm). To evaluate the relative phase shift in the reference beam (introduced by the grating displacement), we measured the positions of the peak intensities along a horizontal line at the middle of the patterns (traced as dashed lines). The measured peak positions in pixels are $[2 \quad 73 \quad 145 \quad 215]$ for the pattern in Fig. 3(a) and $[19, 92, 163, 235]$ for the pattern in Fig. 3(b). With these peak positions we determined that the average displacement of peaks in the second pattern is 18.5 pixels, whereas one quarter of the average period (along the horizontal axis) is 17.875 pixels. The error obtained when these lengths are compared is less than one pixel of the CCD. Thus, the phase shift is close to $\pi/2$, with an error that is within the limits imposed by the CCD resolution.

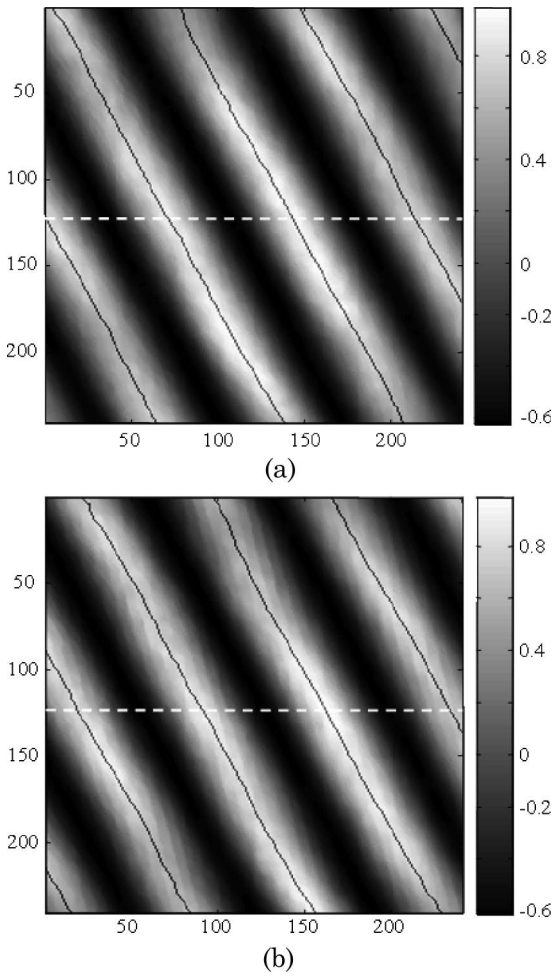

Fig. 3. Interference patterns obtained when both the object and the reference beams are plane waves. These patterns were obtained when the loaded gratings were those depicted in Fig. 2.

As sample objects we employed a deteriorated array of microlenses and a plate containing a bleached bar test pattern. The samples, which were placed at a distance of approximately 17 mm from the CCD plane, were illuminated by a uniform section of the expanded and collimated laser beam. The reference beam, appropriately expanded and collimated, illuminates the CCD area almost uniformly. The normalized real values of holograms $I_c(x,y)$ and $I_s(x,y)$ [Eqs. (8) and (9)] for the array of microlenses, obtained with phase shifts $\delta = 0$ and $\delta = \pi/2$, are shown in Fig. 4. The computed Fourier spectrum modulus of complex field $I_L(x,y) = I_c(x,y) + iI_s(x,y)$ is partially shown in Fig. 5. It is noted, using Eq. (10), that the Fourier spectrum of $I_L(x,y)$ is given by $\tilde{o}(u+u_0, v+v_0)$, which corresponds to the Fourier spectrum of object field $o(x,y)$, centered at the spatial frequency coordinates $(-u_0, -v_0)$. The origin $(0,0)$ in the Fourier spectrum of $I_L(x,y)$, which is easily found in the discrete Fourier transform operation, is identified by the small white cross in Fig. 5. The Fourier spectrum in Fig. 5 is formed by a periodic array of bright spots that are due to the periodicity of the object under study. The small shift of this array with respect to origin $(0,0)$ is due to the linear phase shift $\exp[i2\pi(u_0x + v_0y)]$ in the reference wave [Eq. (6)]. In this particular experiment, coordinates $(-u_0, -v_0)$ are identified at the brightest point of the closest spot to the origin, which is marked in Fig. 5 by the small white arrow. This choice is based on the fact that the tilt introduced in the reference wave was very small. Spatial frequencies $(-u_0, -v_0)$ were obtained by taking into consideration the resolution in this spectrum given by Δx^{-1}, where Δx is the lateral size of the matrix that contains the discrete values of function $I_L(x,y)$. Using these computed spatial frequencies we obtained the linear phase shift $\exp[i2\pi(u_0x + v_0y)]$ that is required to obtain the complex field $o(x,y)$ expressed in Eq. (10). This $o(x,y)$ field is backpropagated to the object plane by use of the exact angular spectrum method. A portion of the wrapped object phase obtained with this propagation, depicted in Fig. 6, shows the phases of microlenses with different degrees of deterioration. The corresponding unwrapped object phase relief is displayed in the three-dimensional plot of Fig. 7. Most of the irregular artifacts observed in the reconstructed phase correspond to deteriorated features of the tested lenslet array. Other artifacts correspond to defects in the

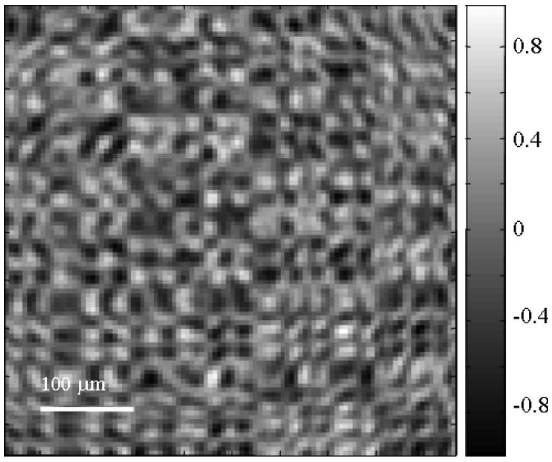

(a)

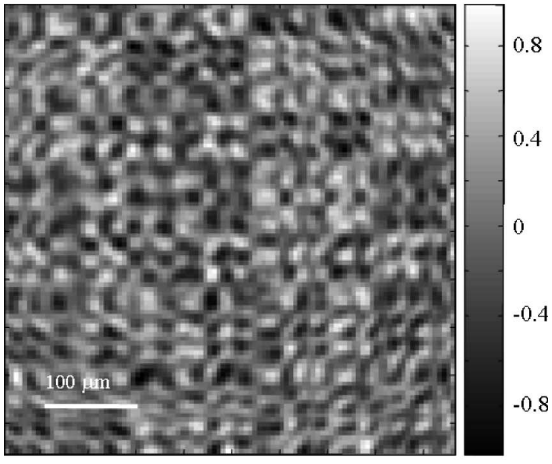

(b)

Fig. 4. Partial views of holograms (a) $I_c(x,y)$ and (b) $I_s(x,y)$ obtained with the array of microlenses employed as the sample object.

unwrapping process and deficiencies in the registration of holograms, which was not optimized. In the experimental result shown in Fig. 7, we estimated

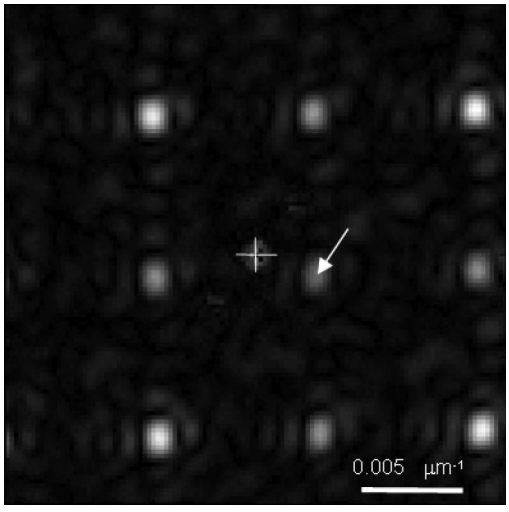

Fig. 5. Modulus of the computed Fourier spectrum of the function $I_L(x,y) = I_c(x,y) + iI_s(x,y)$ obtained for the array of microlenses.

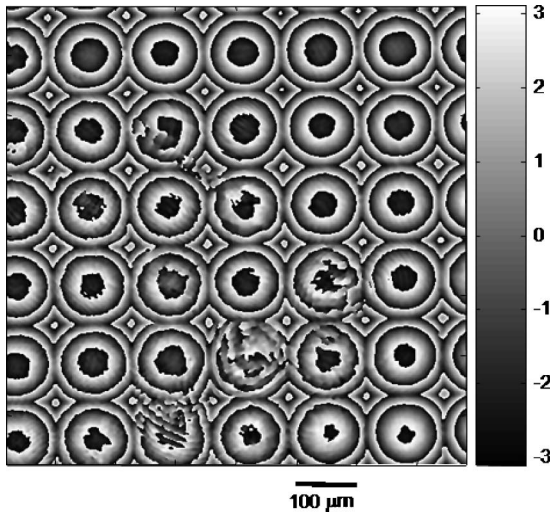

Fig. 6. Wrapped phase of the reconstructed array of microlenses.

a total phase delay of microlenses of approximately 20 rad and a lens width of 127 μm. With these parameters we computed a focal length close to 2 mm, which approximately coincides with the directly measured focal distance. The recording and reconstruction were also performed for a bleached bar test pattern used as the input object. In this case, the real-valued holograms I_c and I_s, together with the unwrapped phase of the recovered object, are shown in Fig. 8. The result shown in Fig. 8(c) indicates that the phase modulation that results from bleaching the original bar pattern is approximately 12 rad. In both cases, the relatively high resolution of the reconstructed phase objects is obtained by computing and interlacing multiple reconstructions with the direct angular spectrum approach for which different small linear phase shifts are applied to the field $o(x,y)$. As is well known, the spatial resolution for each of these reconstructions is equal to the CCD resolution. The resolution of the reconstructed phases in Figs. 6–8 was improved by a factor of 1/9 with respect to the CCD resolution.

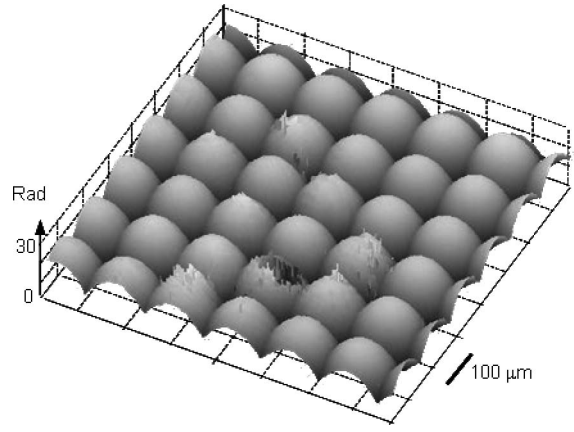

Fig. 7. Three-dimensional representation of the unwrapped phase of the reconstructed array of microlenses.

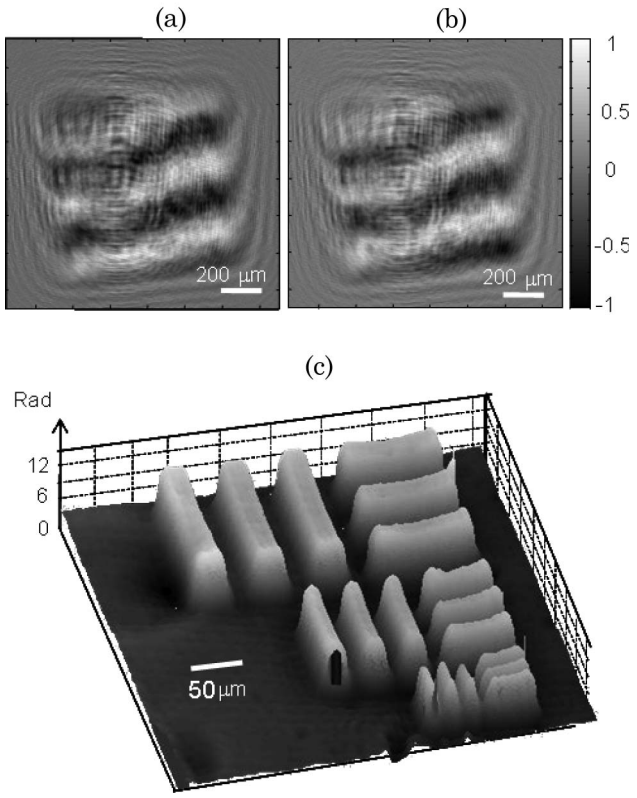

Fig. 8. Normalized real values of holograms (a) $I_c(x,y)$ and (b) $I_s(x,y)$ for the bleached bar test pattern, and (c) corresponding to the three-dimensional image of the reconstructed unwrapped phase of this sample object.

4. Conclusions and Remarks

We have described and experimentally demonstrated a two-step PSI method based on the lateral displacement of a binary grating generated with a TNLC SLM. The demonstration was performed in a Mach–Zehnder DH setup, where the field transmitted by the sample object freely propagates to the CCD plane. The lateral displacement of the grating generated by the SLM is obtained with high accuracy by simply changing the displayed image in this device. Since the generated phase shift depends only on this displacement and not on the exact grating transmittance, the phase shift generated with this method is highly accurate.

We implemented the above method employing a deteriorated array of microlenses and a bleached bar test pattern as sample objects. The reconstruction in the first case, depicted in Figs. 6 and 7, shows the imperfections of the different microlenses in the sample. However, some irregular artifacts in the reconstruction can be due to errors in the unwrapping procedure and to the fact that the electronic register of holograms was not so refined. The detailed analysis of these issues was not developed in this study, which is only aimed as a first demonstration of the proposed PSI method. Nevertheless, the results provide a validation of the proposed PSI technique as a promising method for DH reconstruction of moderately high bandwidth complex fields.

References

1. J. W. Goodman and R. W. Lawrence, "Digital image formation from electronically detected holograms," Appl. Phys. Lett. **11**, 77–79 (1967).
2. M. A. Kronrod, N. S. Merzlyakov, and L. P. Yaroslavskii, "Reconstruction of a hologram with a computer," Sov. Phys. Tech. Phys. **17**, 333–334 (1972).
3. U. Schnars and W. Jüptner, "Direct recording of holograms by a CCD target and numerical reconstruction," Appl. Opt. **33**, 179–181 (1994).
4. E. Cuche, F. Bevilacqua, and C. Depeursinge, "Digital holography for quantitative phase-contrast imaging," Opt. Lett. **24**, 291–293 (1999).
5. E. Cuche, P. Marquet, and C. Depeursinge, "Simultaneous amplitude-contrast and quantitative phase-contrast microscopy by numerical reconstruction of Fresnel off-axis holograms," Appl. Opt. **38**, 6994–7001 (1999).
6. U. Schnars, "Direct phase determination in hologram interferometry with use of digitally recorded holograms," J. Opt. Soc. Am. A **11**, 2011–2015 (1994).
7. T. M. Kreis, "Frequency analysis of digital holography," Opt. Eng. **41**, 771–778 (2002).
8. L. Xu, J. Miao, and A. K. Asundi, "Properties of digital holography based on in-line configuration," Opt. Eng. **39**, 3214–3219 (2000).
9. I. Yamaguchi and T. Zhang, "Phase-shifting digital holography," Opt. Lett. **22**, 1268–1270 (1997).
10. T. Zhang and I. Yamaguchi, "Three-dimensional microscopy with phase-shifting digital holography," Opt. Lett. **23**, 1221–1223 (1998).
11. F. Dubois, C. Minetti, O. Monnom, C. Yourassowsky, J.-C. Legros, and P. Kischel, "Pattern recognition with a digital holographic microscope working in partially coherent illumination," Appl. Opt. **41**, 4108–4119 (2002).
12. P. Guo and A. J. Devaney, "Digital microscopy using phase-shifting digital holography with two reference waves," Opt. Lett. **29**, 857–859 (2004).
13. D. Kim and B. Javidi, "Distortion-tolerant 3-D object recognition by using single exposure on-axis digital holography," Opt. Express **12**, 5539–5548 (2004).
14. B. Javidi and E. Tajahuerce, "Three-dimensional object recognition by use of digital holography," Opt. Lett. **25**, 610–612 (2000).
15. C. Guo, L. Zhang, H. Wang, J. Liao, and Y. Zhu, "Phase-shifting error and its elimination in phase-shifting digital holography," Opt. Lett. **27**, 1687–1689 (2002).
16. G. Popescu, L. P. Deflores, J. C. Vaughan, K. Badizadegan, H. Iwai, R. R. Dasari, and M. S. Feld, "Fourier phase microscopy for investigation of biological structures and dynamics," Opt. Lett. **29**, 2503–2505 (2004).
17. Y. Takaki, H. Kawai, and H. Ohzu, "Hybrid holographic microscopy free of conjugate and zero-order images," Appl. Opt. **38**, 4990–4996 (1999).
18. V. Arrizón and D. Sánchez-de-la-Llave, "Common-path interferometry with one-dimensional periodic filters," Opt. Lett. **29**, 141–143 (2004).
19. C. Meneses-Fabian, G. Rodriguez-Zurita, and V. Arrizón, "Optical tomography of transparent objects with phase-shifting interferometry and stepwise-shifted Ronchi ruling," J. Opt. Soc. Am. A **23**, 298–305 (2006).